



1 **Ice core nitrogen isotopes archive dramatic changes in West Antarctic  
2 Ice Sheet thinning**

3  
4 Amy C. F. King<sup>1</sup>, Thomas K. Bauska<sup>1</sup>, Amaëlle Landais<sup>2</sup>, Carlos Martín<sup>1</sup>, Eric W. Wolff<sup>3</sup>

5  
6 <sup>1</sup> British Antarctic Survey, High Cross, Madingley Road, Cambridge, CB3 0ET, United Kingdom

7 <sup>2</sup> Laboratoire des Sciences du Climat et de l'Environnement, LSCE/IPSL, CEA-CNRS-UVSQ, Université Paris-Saclay, Gif-  
8 sur-Yvette, France

9 <sup>3</sup> Department of Earth Sciences, University of Cambridge, Downing Street, Cambridge, CB2 3EQ, United Kingdom

10 *Correspondence to:* Amy C. F. King (amyking@bas.ac.uk)

11  
12  
13  
14  
15  
16  
17  
18  
19  
20  
21  
22  
23  
24  
25  
26  
27  
28  
29  
30  
31  
32



33 **Summary**

34 We show how measurements of nitrogen isotopes in Antarctic ice core records can be used to show dramatic thinning of an  
35 ice sheet during ice mass changes in the Holocene. Combining such measurements with proxies for ice sheet elevation could  
36 be a powerful tool for constraining the history of ice dynamics at sites which are sensitive to rapid changes, and could contribute  
37 to constraining ice sheet models.

38 **Abstract**

39 The behaviour of ice sheets during ice mass loss is currently not well constrained and is a major limiting factor in accurate  
40 predictions of ice sheet behaviour in our warming climate. Proxies from ice cores can record the history of ice mass loss at  
41 exceptional temporal resolution and unrivalled chronological accuracy. A recent record of Total Air Content (TAC) and ice  
42 core chemistry from Skytrain Ice Rise resolved a 450 m drop in ice sheet elevation at the site in the Weddell Sea Sector of the  
43 Antarctic Ice Sheet 8,000 years ago, an event which occurred over just 200 years. The event is thought to represent an  
44 ungrounding and removal of the buttressing effect on the ice sheet in the region. However, proxy records for ice elevation,  
45 TAC, can show unexpected signals which indicates an imperfect understanding of how such gas records are captured in ice  
46 cores during rapid changes in ice sheet conditions, inhibiting expansion of such studies to other sites. Here we use ice core  
47 nitrogen isotope measurements to elucidate the dynamic evolution of the firn column, where such gas records are gradually  
48 trapped, during the 8 ka rapid ice mass loss. The horizontal divergence imparted on the ice rise during the event dramatically  
49 thinned the firn column to the extent that dynamic thinning of the firn is the dominating factor in how nitrogen isotopes are  
50 captured. As a result, the recorded signal of nitrogen isotopes directly opposes the signal predicted by current firn models  
51 which do not include such ice dynamics, suggesting that it is a critical factor to include in firn modelling studies of sites  
52 susceptible to rapid ice mass changes. Our findings allow us to tightly constrain where reliable elevation signals, not disrupted  
53 by changing ice dynamics, are available in ice core records. Moreover, our study demonstrates that the combination of TAC  
54 and nitrogen isotopes can be a powerful tool in constraining ice sheet dynamics at a site, thus helping to inform the physics of  
55 ice sheet models.

56

57

58

59

60

61



## 62 1 Introduction

63 Uncertainty in ice sheet processes is identified as one of the major limiting factors in accurately predicting future sea level rise  
64 under current emissions pathways (Pörtner et al., 2022). Under all current scenarios, the West Antarctic Ice Sheet (WAIS) is  
65 shown to be one of the most decisive climate tipping elements due to its high sensitivity to temperature increases and  
66 subsequent effects on sea level (Rosser et al., 2024). It is thus critical that we improve our understanding of both the timing  
67 of, and mechanisms behind, ice mass loss in this region. An effective way to do this is to obtain high resolution records of past  
68 ice sheet behaviour, which can be used to inform the models that predict future ice mass changes.

69

70 Ice cores provide exceptional records of past ice sheet behaviour, capturing direct samples of the ice properties and the  
71 atmosphere at the time the ice formed. A recent study from an ice core drilled at Skytrain Ice Rise (SIR) (Grieman et al., 2024)  
72 (Fig. 1) combined multiple ice-core climate proxies to elucidate ice sheet changes in the Weddell Sea region throughout the  
73 Holocene deglaciation. The study observed a rapid decline in ice mass at the ice core site approximately 8,000 years ago (8  
74 ka), with a 450 m reduction in ice sheet elevation over just 200 years, imposed on a background of more gradual ice mass  
75 decline. The event was followed by substantial ice shelf retreat in front of the ice rise. The proposed mechanism behind such  
76 a rapid ice mass loss was that ungrounding of the ice sheet at the ice/ocean margin, with ocean water encroaching underneath  
77 the ice sheet. The sudden loss of the buttressing effect of the grounded ice that would otherwise have constrained outward flow  
78 of the ice sheet drove a rapid thinning upstream of the grounding line and Skytrain Ice Rise experienced a drop in elevation.  
79 This is the first time such a rapid, centennial scale ice-loss event has been so well resolved in a direct climate record, and it  
80 raises important questions as to the potential for such future events to occur in other regions where ice currently grounded on  
81 retrograde slopes – most notably the Amundsen Sea region and Thwaites Glacier. We would thus look to repeat such studies  
82 in other ice core records throughout the region and indeed more widely through the ice sheet to help improve the spatial and  
83 temporal resolution of our picture of such rapid ice mass loss. However, a key record used to reconstruct the past elevation of  
84 the ice sheet in the study, the Total Air Content (TAC) of ice core samples, showed a complex oscillating signal throughout  
85 the period of rapid ice mass loss (Fig. 1) which cannot be directly attributed to elevation change (Grieman et al., 2024) but is  
86 a real signal recorded in the ice well above the threshold of our high-accuracy TAC method (Nehrbas-Ahles et al., 2022). An  
87 improved understanding of the parameters affecting the TAC signal, and more widely the capture of gases in ice core samples  
88 during rapid ice sheet changes, is required before the study can be expanded.

89

90 One underexplored process is the effect of ice sheet thinning on gas record preservation. In the case of TAC, physical properties  
91 of the firm column (the upper snow layers where compaction from snow to ice is in process and has not fully isolated the air  
92 bubbles from the overlying surface air) such as temperature and pore volume (the space available between snow grains in the  
93 firm column) affect the total amount of gas captured (Martinerie et al., 1992). Changes in the firnification processes thus have  
94 the potential to greatly impact TAC and other gas record capture. Thinning, or horizontal divergence, is often ignored in firm



95 studies and infrequently discussed as a possible driver of variability in gas-phase proxies, with the notable exception of thinning  
96 changing the firn temperature gradient at South Pole (Morgan et al., 2022). This stems from the fact that most ice cores are  
97 drilled into some of the thickest areas of the ice sheet (> 3,000 meters depth) and thus thinning in the firn (the uppermost 50  
98 to 100 meters) is relatively minor. In contrast, SIR is only 650 meters thick with a firn column of at least 50 meters.  
99 Additionally, as SIR is frozen to the bed, the ice flow in the lowermost hundred meters or so is very slow and thus most of the  
100 thinning occurs in a relatively short column of the uppermost ice. Furthermore, we typically drill ice cores on thick, stable  
101 domes or divides that do not record any major flow disturbances or changes in ice thickness. Even a record like WAIS Divide,  
102 an ice core drilled in central West Antarctica, has probably only experienced modest changes in elevation during the last  
103 deglaciation, on the order of few hundred meters, which is relatively minor compared to total ice thickness (~10% of a total of  
104 ~3,450 meters). In contrast, SIR is currently 650 meters thick but may have been up to 1,300 meters thick prior to the rapid  
105 ice loss at 8 ka. The ice thinned by up to 650 meters (most likely value being 450 meters) (Grieman et al., 2024), meaning that  
106 potentially the whole column thinned by up to 50% within just a few hundred years.

107  
108 Secondly, accumulation-induced thinning driven simply by the vertical motion of ice is relatively minor at most sites. For  
109 example, a typical core in East Antarctica might have an accumulation rate of  $0.05 \text{ m a}^{-1}$  over a thickness of 3,000 meters,  
110 which gives a whole column horizontal divergence of  $\sim 2 \times 10^{-5} \text{ a}^{-1}$ , where horizontal divergence is approximately equal to  
111 accumulation divided by ice thickness (see Equation 3). Meanwhile, SIR, with modest accumulation at  $0.14 \text{ m a}^{-1}$  and ice  
112 thickness of only 650 meters, experiences nearly an order of magnitude faster rates of thinning ( $\sim 2 \times 10^{-4} \text{ a}^{-1}$ ).

113 In this study we use nitrogen isotopes to determine the changing properties of the firn column during rapid loss of ice sheet  
114 elevation at SIR. The ratio between nitrogen isotopes  $^{15}\text{N}$  and  $^{14}\text{N}$ , expressed herein as  $\delta^{15}\text{N}$ , is constant in the atmosphere over  
115 the timescales we consider here, and so any change in the ratio is due to fractionation processes in the firn column  
116 (Severinghaus et al., 2003). These may be preferential gravitational settling of the heavy isotope, telling us the thickness of the  
117 firn column, or preference of the heavier isotope toward cold temperatures, which tells us about the temperature fluctuations  
118 within the firn column. We combine these measurements with firn modelling techniques to show how  $\delta^{15}\text{N}$  can tell us about  
119 dramatic changes in ice sheet thickness. We also identify potential missing processes in our current understanding of the  
120 firnification process at the ice core site. We conclude by proposing the mechanisms behind the disrupted TAC gas archive in  
121 Skytrain ice core and add to the picture of the processes occurring in the ice sheet at SIR during rapid ice mass loss.

## 122 2 Methods

### 123 Skytrain Ice Core Sampling

124 The 651 m Skytrain ice core was drilled at Skytrain Ice Rise during the field season 2018-2019 (Mulvaney et al., 2021).  
125 Samples for nitrogen isotope analysis were selected based on the previously developed ST22 age scale (Hoffmann et al., 2022;



126 Mulvaney et al., 2023). To align with previously published TAC data, sample ages are presented on the ST22-WD2014 version  
127 of the gas age scale, where age alignment has been optimised to the WD2014 age scale. Sampling in this study covers the  
128 period of disrupted TAC signal around the 8 ka elevation change as well as a period of relative TAC stability on either side. A  
129 total of 60 samples were taken between 352.0 – 403.35 m, representing an age range of 5.84 – 8.54 ka, and giving an average  
130 age resolution of 46 yrs. Samples of 5 cm length were taken from a pre-cut ice strip of 3.2 x 3.2 cm, from which the previously  
131 measured TAC samples had also been taken. Samples for nitrogen isotopes were taken proximally (or as close to, dependent  
132 on features such as cracks) to where TAC samples had been taken to allow for close replication. Samples were prepared in the  
133 -25°C cold laboratories at the British Antarctic Survey, Cambridge, UK, and transported to the analytical laboratory in Paris,  
134 France, in insulated boxes and using specialist cold chain shipping which retains sample temperature at -25°C.

### 135 **Nitrogen Isotope Analysis**

136 Nitrogen isotopes, alongside argon isotopes and the ratio of O<sub>2</sub>/N<sub>2</sub>, were measured at LSCE, Paris. After removing 2-3 mm of  
137 the exterior part of the ice samples, air was extracted from the ice samples using a semi-automatic melt - refreeze line. Three  
138 duplicate samples can be processed each day together with two samples of outside air used for daily calibration. In short, the  
139 samples are placed into glass vessels which are evacuated before the ice is melted, enabling air to escape from the bubbles.  
140 The melt water is then refrozen, and the extracted air is cryogenically trapped in tubes filled with silica gel and immersed in  
141 liquid nitrogen. After 3 hours at 30°C, allowing air desorption from the silica gel, the air is introduced into the bellows of an  
142 isotopic ratio mass spectrometer (Thermo® Delta Q). The isotopic and elemental measurements are performed by dual inlet,  
143 i.e. by successive introduction of a small amount of the sample and the measurements standard (dry air without CO<sub>2</sub>). Two  
144 sequences of 16 dual inlet measurements are performed, usually leading to a 1-sigma uncertainty of 0.007 ‰ and 0.6 ‰  
145 respectively for δ<sup>15</sup>N and δO<sub>2</sub>/N<sub>2</sub>. For the Skytrain samples, the values for the 1-sigma uncertainty were larger (0.14 ‰ for  
146 δ<sup>15</sup>N and 1.8 ‰ for O<sub>2</sub>/N<sub>2</sub>) suggesting variability at short spatial scale in this record. Although less precise than with other  
147 techniques using purification of the gas (Servettaz et al., 2022), δ<sup>40</sup>Ar can also be measured with this configuration of the Delta  
148 Q mass spectrometer. There was a 1-sigma uncertainty of 0.06 ‰ for δ<sup>40</sup>Ar on this series of measurements.

149  
150 Final values of δ<sup>15</sup>N and δ<sup>40</sup>Ar preserved in the ice core are products of both thermal and gravitation fractionation within the  
151 firm column. Following Severinghaus et al. (2003) the difference in mass dependent gravitation fractionation between the two,  
152 which is four times greater for δ<sup>40</sup>Ar, can be used to isolate the thermal component of the signal, N excess.

153  
154 *Equation 1*

155 
$$N_{excess} = \delta^{15}N - (\delta^{40}Ar/4)$$

156



157 A negative N excess value implies that the top of the firn column was colder than the base, and a positive N excess implies the  
158 top of the firn column was warmer than the base. Using the thermal sensitivities of N ( $\Omega_N$ , 0.0145  $\text{‰}^{\circ}\text{C}^{-1}$ ) and Ar ( $\Omega_{\text{Ar}}$ , 0.036  
159  $\text{‰}^{\circ}\text{C}^{-1}$ ) we can deduce the temperature difference in the firn,  $\Delta T$ .

160

161 *Equation 2*

162

$$\Delta T = \frac{N_{\text{excess}}}{\Omega_N - (\Omega_{\text{Ar}}/4)}$$

163 **Sample Gas Fractionation**

164 Loss of gases from ice core samples can cause distortion of the captured gas records. Gas fractionation processes can occur  
165 during bubble formation or due to post-coring factors (Bender et al., 1995). Smaller gas molecules can more easily diffuse out  
166 of the ice compared to larger molecules, thus gas fractionation can be indicated using the ratio of O<sub>2</sub>, the smaller molecule, to  
167 N<sub>2</sub>, the larger molecule in the ice core samples. The record of O<sub>2</sub>/N<sub>2</sub> for Skytrain shows no change above the background  
168 variability of the data in the period measured (Supplement Figure 2).

169 **Community Firn Model**

170 We employed the Community Firn Model (CFM) (Stevens et al., 2020) as a heuristic guide to understand the processes driving  
171 the  $\delta^{15}\text{N}$  variability we observe, as well as a quantitative method to explore possible histories of temperature, accumulation  
172 and ice sheet thinning that reconcile our  $\delta^{15}\text{N}$  data. The CFM is an open-source firn model designed to simulate the evolution  
173 of physical firn properties such as temperature, density, porosity, and associated firn air parameters including profiles of  $\delta^{15}\text{N}$   
174 and  $\delta^{40}\text{Ar}$  (thus N excess is modelled). Here we present results that were run exclusively in the standard physics setup which  
175 enables a transient evolution of the Herron and Langway (1980) empirical model (“HLdynamic”) with ice conductivity based  
176 on Calonne et al. (2019)

177 Additionally, we use the recently developed horizontal divergence scheme in the CFM (Horlings et al., 2021) whereby a parcel  
178 (in a Lagrangian framework) is first compressed due to densification and then further thinned due to a prescribed horizontal  
179 divergence rate. In our case, we impose a total horizontal divergence rate ( $a^{-1}$ ). To calculate the total horizontal divergence, we  
180 sum the divergence imparted from accumulation  $a$  (m  $a^{-1}$ ) and rate of change in ice sheet thickness  $\dot{H}$  (m  $a^{-1}$ ):

181 *Equation 3*

182

$$\dot{\epsilon}_h = \frac{a}{H} + \frac{\dot{H}}{H}$$

183



184 By dividing the vertical velocity induced by both accumulation and change in ice sheet thickness by the ice sheet thickness  
185 itself ( $H$ ) we are assuming that ice is incompressible, and more importantly that the vertical strain is uniform in the ice column.  
186 The uniform strain is an oversimplification, but a conservative one. If the ice sheet is frozen to the bed, as is the case with SIR,  
187 the vertical velocity slows dramatically near the base of the ice sheet. Typically, this is at least one hundred meters off the bed  
188 and thus the effective value of  $H$  one might consider to calculate horizontal divergence is some fraction of the true thickness.  
189 A more accurate method using a Lliboutry vertical profile (Lliboutry, 1979) is employed in our 1-D borehole model, but to  
190 first order our approximation is sufficient for our heuristic purposes.

191

192 Another crucial assumption of our model is that the material properties of the firn do not change with the imposed thinning.  
193 For example, there is no further change in density nor any feedback into the densification rate itself such as strain-induced  
194 softening (Oraschewski and Grinsted, 2022) – a set of assumptions that may require further study. The net effect of enhanced  
195 horizontal divergence is a shoaling of the close-off depth, as has been shown to be important in fast-flowing ice regimes, not  
196 unlike SIR during a rapid thinning event.

197

198 To drive the CFM in all the heuristic experiments (Fig. 2), we use the stable water isotopes records to first derive a plausible  
199 surface temperature history of the site using an isotope-to-temperature conversion of 0.8 per mil per deg C with a modern  
200 temperature (last 250 years) of -25°C. To roughly estimate an accumulation history we then use a temperature-dependent  
201 accumulation rate conversion of 0.005 m ice equivalent per deg C (about 3.3% per deg C) with a modern accumulation of 0.15  
202 m ice equivalent. This choice of sensitivity places the accumulation rate increase at 8 ka between the prior and posterior  
203 histories from the Skytrain chronology (Supplementary Figure 5). Additionally, this sensitivity is within bounds but at the  
204 lower end of model- and data-based constraints on the Antarctic-wide accumulation-to-temperature relationship (Nicola et al.,  
205 2023)

206

207 As a first pass constraining a possible thinning history, we extracted the ice thickness history at SIR from a single experiment  
208 with the Parallel Ice Sheet Model (PISM) model and calculated the thinning-induced divergence rate. The particular transient  
209 experiment comes from the deglacial scenario presented in Kingslake et al. (2018) which indicated a widespread retreat of the  
210 grounding line starting around 12,500 years before present that extended further inland than the present-day grounding line  
211 before readvancing in the early Holocene. The absolute timing, rate of change and magnitude of this response in the model  
212 have been shown to be dependent on model boundary conditions and parameterization - in particular model resolution and bed  
213 topography (Albrecht et al., 2020b, a). For consistency with previous work (Grieman et al., 2024) we use this particular model  
214 and align the elevation drop with the initial rise in water isotopes at 8 ka by shifting the modelled time forward by 4,500 years.  
215 We stress that this model run is only a guide to the possible divergence rates and that the detailed history of WAIS retreat  
216 remains highly under constrained from models alone.



217 **Smoothing Splines**

218 Smoothed splines of datasets are generated using the methods presented in King et al. (2024). Briefly, the method applies a  
219 random sampling with replacement bootstrap over 10,000 iterations with the smoothing function generating a spline and  
220 uncertainty bands based on the smoothing parameter. The parameter is tuned to the time-resolution and length of the input data  
221 such that the spline produced is at half height of a generic cosine function, which is a good balance point between preserving  
222 signals in the record while not being overly influenced by record variability. Spline parameters used for each dataset can be  
223 found in Supplement Table 1.

224 **3 Results and Discussion**

225 **Modelling drivers of  $\delta^{15}\text{N}$  change**

226 As a first step, we use the CFM to break down the possible drivers of  $\delta^{15}\text{N}$  change at SIR into constituent parts in a series of  
227 factorial experiments. These experiments should not be considered perfect reconstructions of individual factors as the forcings  
228 (temperature, accumulation and thinning) are not known *a priori*, but rather illustrations to guide us. First, holding all other  
229 variables stable, we change surface temperature (Fig. 2, Scenario 1), increasing it by about 4°C which roughly reflects the  
230 lapse-rate impact of the reconstructed decrease in elevation at 8 ka. The result is an initial increase in  $\delta^{15}\text{N}$  as a strong  
231 temperature gradient is briefly established in the firn and the thermal fractionation dominates, followed by a shift toward  
232 slightly lower values as the firn densification adjusts to the warmer temperature and the close-off depth shoals. In the second  
233 experiment, Scenario 2, we change only accumulation, increasing it as would be expected from an ice core site experiencing  
234 warmer, more moist, more coastal conditions. Here the close-off depth increases along-side the  $\delta^{15}\text{N}$ . In the third experiment,  
235 Scenario 3, we combine both temperature and accumulation and see how competing effects of temperature and accumulation  
236 on close-off depth largely cancel each out and the thermal effect (the peak in  $\delta^{15}\text{N}$ ) dominates the signal. At the same time, the  
237 bubble close-off depth becomes slightly shallower, from ~58 m to ~52 m. The result is a predicted peak at ~8.0 ka, with  
238 increases in both  $\delta^{15}\text{N}$  and N excess (Supplement Fig. 2) of ~0.04 ‰ and ~0.02 ‰ respectively, which decay away by ~7.8  
239 ka.

240 This suggests that all else being equal, we would expect to see a peak in  $\delta^{15}\text{N}$  across the 8 ka event. However, as we will see,  
241 this is not the case.

242 To explore a new scenario, in the fourth experiment (Scenario 4) we model just changes in horizontal divergence as modelled  
243 in the PISM simulation (see methods) combined with a small, constant divergence induced by the relatively high accumulation  
244 in a short ice column. The increased divergence causes the close-off depth to shoal and the  $\delta^{15}\text{N}$  decreases strongly as the



245 gravitational effect dominates the signal. We thus have a competing effect from thinning that could potentially drive the  $\delta^{15}\text{N}$   
246 signal.

247 **Comparing  $\delta^{15}\text{N}$  model predictions and measured data**

248 We now compare our predictions to the measured data (Fig. 3). Comparing  $\delta^{15}\text{N}$ , where each of our temperature and  
249 accumulation scenarios predict a peak in values, we observe a similar small initial peak, from a spline-based value of  $0.20 \pm$   
250  $0.01 \text{‰}$  at 8.4 ka to  $0.22 \pm 0.006 \text{‰}$  at 8.1 ka. However, this is followed by a large decrease in  $\delta^{15}\text{N}$  to a minimum of  $0.13 \pm$   
251  $0.008 \text{‰}$  at  $\sim 7.4 \text{ ka}$ . The minimum is reached approximately 500 years after the initiation of ice mass changes at SIR, with a slow  
252 recovery in values lasting until  $\sim 6.6 \text{ ka}$  with values of  $0.22 \pm 0.007 \text{‰}$ , and with an apparent slow reduction and ‘re-  
253 stabilisation’ of values to  $0.19 \pm 0.007 \text{‰}$  by  $\sim 6 \text{ ka}$ . This indicates that after an initial as-predicted reaction to increasing  
254 temperature and accumulation at the site as elevation lowered, the horizontal divergence factor takes over with a striking  
255 dominating effect on the firn signal of  $\delta^{15}\text{N}$ . The dynamic ice changes at SIR appear to last up to a duration of 1,500 years  
256 following the start of the initial rapid 200-year event of ice elevation loss as observed in Grieman et al. (2024).

257 Predicted values of N excess are also contradicted by the measured data. Again, a small increase in N excess is predicted in all  
258 scenarios at the initiation of ice mass change 8 ka, returning to stable values shortly thereafter. Despite a large scattering, our  
259 results suggest that values first increased to a spline-based value of  $-0.02 \pm 0.004 \text{‰}$  at  $\sim 8 \text{ ka}$  from  $-0.03 \pm 0.004 \text{‰}$  at  $\sim 8.4$   
260 ka, and then reduced to as low as  $-0.04 \pm 0.004 \text{‰}$  at  $\sim 7.5 \text{ ka}$ . Measured N excess data shows that values remain negative  
261 throughout, with a reduction towards more negative values occurring throughout the same period as the reduced  $\delta^{15}\text{N}$ .

262 Comparing both  $\delta^{15}\text{N}$  and N excess to the TAC signal (Fig. 3), the disruption to the signals, with lowering of values and  
263 recovery, spans the full duration of the oscillating TAC signal, with a minimum duration of  $\sim 1,500 \text{ years}$ .

264 **Optimising model-data agreement**

265 So far we have considered the importance of individual factors in explaining our nitrogen isotope records. We now attempt  
266 to ‘tune’ the model output to the best fit for our measured  $\delta^{15}\text{N}$  and explore some plausible scenarios that may best explain  
267 our measured record (Fig. 4). The most realistic starting point from our factorial experiments is a combination of Scenarios 3  
268 and 4, including the changes in temperature, accumulation rate and horizontal divergence. While this combination comes  
269 close to explaining our  $\delta^{15}\text{N}$  record, it predicts absolute values of  $\delta^{15}\text{N}$  which are slightly higher than the measured data both  
270 preceding and during the drop in  $\delta^{15}\text{N}$ , and a drop and recovery in  $\delta^{15}\text{N}$  values which is slightly shorter in duration than  
271 suggested by the measured data (Fig. 4, ‘Combined Scenario’).

272 One possibility to align absolute values of the  $\delta^{15}\text{N}$  is to consider a stronger, two-phase increase in accumulation following  
273 the water isotope increase. Grieman et al. (2024) argued that delays in the Na increase relative to the water isotope increase



274 reflects that thinning preceded ice shelf breakup. The proposed breakup phase centres around 7.5 ka, which aligns with an  
275 increase in  $\delta^{15}\text{N}$  not captured in our idealized scenario. Following ice shelf breakup Skytrain Ice Rise would be  
276 approximately 270 km closer to local sources of moisture, which could have increased accumulation. In the optimized  
277 scenario we include a second increase in accumulation after 7.5 ka which drives a stronger, sharper increase in  $\delta^{15}\text{N}$  as the  
278 thinning returns to steady-state. This larger increase in accumulation before and after the jump with an effective  
279 accumulation-to-sensitivity of approximately 6% also improves the  $\delta^{15}\text{N}$  match before and after the jump – which are nearly  
280 equal in the data.

281 Additionally, our idealized scenario assumes uniform strain throughout the ice column whereas, in reality, thinning rates will  
282 be higher in the upper sections. To better fit the shape of the drop in the measured  $\delta^{15}\text{N}$ , we require the firn column to be  
283 thinned for a longer duration than that suggested by the current model and with a marginally higher divergence rate.  
284 Although this is a subjective process, we increase the duration over which the horizontal divergence is acting on the firn in  
285 the model and increase the divergence rate to within a reasonable fit of the measured data to give a suggestion of the  
286 magnitude of change required. This is not intended to be quantitative but does suggest that the ice thinning at SIR in the  
287 PISM model may be underestimated in both duration and magnitude. Further quantification would require extracting the  
288 thinning rates from a 3D thermo-mechanical ice sheet model, but in principle this demonstrates that ice core nitrogen  
289 isotopes can inform the physics of the ice sheet models.

## 290 **N excess as a temperature signal at Skytrain**

291 Is our N excess record a signal of firn column temperature? If we take the N excess as a true indication of firn column  
292 temperature, then our data rather surprisingly suggests that the top of the firn column cooled relative to the base of the firn  
293 column,  $\Delta T$ , by up to  $-4\text{ }^{\circ}\text{C}$  (Supplement Fig. 1). Given the observed rise in site temperature and accumulation rate following  
294 surface lowering of the ice sheet, this is unexpected. The pre-existing gradient of warming down the borehole at SIR (shown  
295 on Supplementary Fig. 2) comes from the geothermal gradient of the ice at the site (Mulvaney et al., 2021). An increasingly  
296 negative N excess signal would require a relative cooling of the surface air at the site or a relative warming of the base of the  
297 firn column. In the case of the former, we already know that the surface elevation lowered and surface temperatures  
298 subsequently increased. A possible mechanism for warming the base of the firn column exists where thinning of the ice sheet  
299 occurs at a site where a geothermal gradient warms the base of the ice sheet upwards, or where the geothermal heat flux itself  
300 increases. The latter we rule out over the timescales and magnitude of temperature change required here. Considering the  
301 former, at the Skytrain ice core site, the measured borehole temperature profile shows an increase in temperature down through  
302 the depth of the ice sheet due to the geothermal gradient, from a modern surface temperature of  $-26\text{ }^{\circ}\text{C}$  to a basal temperature  
303 of  $-15\text{ }^{\circ}\text{C}$ , a  $-11\text{ }^{\circ}\text{C}$  change over the 654 m ice thickness. Though a potential mechanism to warm the base of the firn column,  
304 this would be combined with warming surface temperatures, reducing the temperature gradient in the firn column. While the  
305 required temperature gradients for our N excess data seem unlikely in these scenarios, we briefly test these assumptions



306 employing a 1D borehole thermal model (see Supplement). Given the known physical properties at the site, the model confirms  
307 that an inversion of temperature gradient to more negative values at the top of the firn column did not occur (Supplement Fig.  
308 2).

309

310 We did not use the most optimised methodology for measurement of  $\delta^{40}\text{Ar}$  on these samples as the main target was  $\delta^{15}\text{N}$ . This  
311 introduces a limit on how far we can interpret the  $\delta^{40}\text{Ar}$  and as such the N excess signals, alongside the higher 1-sigma  
312 uncertainty of the samples suggesting short term variability in the Skytrain record.

### 313 **Comparison to other ice core records**

314 A similar example in terms of magnitude and duration of the nitrogen isotope records observed in Skytrain is presented in the  
315 literature, in the Siple Dome ice core (Severinghaus et al., 2003). Siple Dome sits at the interface between the Ross Ice Shelf  
316 and WAIS and is similar to Skytrain Ice Rise in location, between ice shelf and ice sheet, in background climatic conditions  
317 in the Holocene, and previous geomorphological evidence of large-scale and rapid loss of ice mass in the Ross Sea region  
318 during the Holocene (Pittard et al., 2022; Spector et al., 2017).

319 At approximately 15 ka,  $\delta^{15}\text{N}$  (Fig. 6) drops rapidly to near zero at Siple Dome. The effect of any thinning in the firn column  
320 at Siple Dome must be even greater than at Skytrain, as the  $\delta^{15}\text{N}$  record suggests that gravitational fractionation, and therefore  
321 diffusive column height, reduced to near zero. Alternatively, there is potential for a process which enhances the effect of the  
322 thinning firn column on the isotope records, for example cracking of the ice exposing gases deeper in the firn column to modern  
323 air.

### 324 **Does ice sheet thinning explain the Skytrain TAC signal?**

325 We now revisit how this new understanding of physical firn column changes can help with our interpretation of the TAC  
326 record observed in the Skytrain ice core. Our isotope records show that the TAC record is disrupted throughout the same time  
327 interval that the firn column is being affected by dynamic changes in firn column thickness. This extends beyond the actual  
328 period of change in elevation of the ice sheet at the ice core site. A reliable elevation record from TAC is thus only available  
329 where physical firn column processes are also stable. Based on this study, we define this period of disruption for the Skytrain  
330 ice core record as between  $\sim 8.2$  ka, before the initial small upward inflection which corresponds to the beginning of the  
331 elevation change, and  $\sim 6.5$  ka, where the  $\delta^{15}\text{N}$  data values re-stabilise and align with model predictions not including horizontal  
332 divergence, suggesting stabilisation of firnification processes at the site. This supports the decision of Grieman et al (Grieman  
333 et al., 2024) to compare only the stable values from 9.5–8.5 ka (before the disruption) and those from 6.6 to 5.0 ka (after the  
334 disruption) to assess the net change in elevation.

335



336 The specifics behind the oscillating signal of TAC during dynamic thinning of the firn column are not explained by our isotope  
337 data. With temperature change at the site well constrained, we must consider the other major influence on TAC, pore volume,  
338 to explain TAC variability. The nitrogen isotope record presents a consistent drop and then recovery of values over the period  
339 of ~ 1.5 kyr, without the oscillations of the TAC record, indicating that the impact on the TAC signal of the thinning of the  
340 firn column is not a simple, linear response to a single factor that could be driven by the dynamic thinning, for example an  
341 artificial decrease in pore volume driven by mechanical deformation of the snow grain structure.

342

343 Pore volume has been shown to be controlled by a complex interplay between the gas and physical ice properties of a firn  
344 column at each ice core site based on varying rates of temperature change, accumulation rate and densification profiles.  
345 However the fine scale controls on TAC are currently under-studied. Epifanio et al. (2023) observed a strong correlation  
346 between accumulation rate and TAC at the low accumulation South Pole ice core site. They propose that snow grain  
347 metamorphism is behind this link, with low accumulation rate allowing grains to grow proportionally larger as they remain on  
348 or close-to the snow surface for longer, as well as growing towards more spherical shapes that promote higher gas diffusivity  
349 and lower TAC. This agrees with Gregory et al. (2014), who found that low accumulation sites in Antarctica close-off at lower  
350 open porosity with higher gas diffusivity, compared to higher accumulation sites with finer grain sizes. They suggest that  
351 layering in the firn column may also control TAC changes, with layers capturing relic microstructures controlled by  
352 accumulation at the time that layer was at the snow surface, which could be a mechanism to control TAC variations over short  
353 timescales. Contrastingly, in a central Greenland core, Eicher et al. (2016) found that higher accumulation may lower TAC.  
354 With TAC being controlled at the point of bubble close-off, higher accumulation would increase the load on the snow surface  
355 and increase densification rates, inhibiting formation of spherical grains and reducing pore volume. This effect could alter the  
356 TAC signal for several hundreds of years following the accumulation increase. None of these sites match the physical ice  
357 properties and meteorological conditions of the Skytrain ice core. However, these examples do show how strongly TAC may  
358 be affected by differing controls on pore volume within a firn column, with such changes being plausible over a rapid ice mass  
359 reduction with dynamic firn column changes.

360

361 The oscillating TAC at Skytrain is likely to be a complex interplay of some or all of the above processes as the ice elevation  
362 loss and dynamic thinning cause disequilibrium of the firnification process. Future work is planned for grain-scale analysis of  
363 Skytrain ice core samples throughout the Holocene TAC record which may help to elucidate the microstructure changes  
364 occurring during the oscillation. We suggest that paired measurements of high-accuracy TAC and inert gas isotopes could be  
365 a powerful tool for constraining the history of ice dynamics at ice core sites – particularly at those sites that are sensitive to  
366 rapid changes in ice sheet configurations. Neither proxy stands on their own as a perfect archive of ice sheet thickness, with  
367 one proxy being obscured or over printed by other processes that are, at least partially, constrained by the other.



368 **4. Conclusions**

369 Nitrogen isotope measurements in Skytrain ice core identify a period of dramatic firn column thinning during a rapid ice  
370 elevation loss at about 8 ka, a process which apparently disrupts the capture of the TAC signal due to the disequilibrium of the  
371 firnification process. As ice mass decreased in the Weddell sector of the WAIS through the Holocene deglaciation,  
372 ungrounding of the ice at the ice margin and removal of the buttressing effect resulted in horizontal divergence in the ice at  
373 Skytrain Ice Rise, thinning the firn column. Such thinning significantly reduces the gravitational fractionation of nitrogen  
374 isotopes in the firn column, dominating the physical factors that influence the isotope signal (temperature, accumulation rate)  
375 and resulting in a drop in  $\delta^{15}\text{N}$  values (Fig. 6). As far as we are aware from existing literature, this is the first time such a  
376 mechanism has been proposed using nitrogen isotope analysis in ice cores. A similar feature is present in the existing Siple  
377 Dome ice core nitrogen isotope record at 15 ka, hinting at the possibility that the same mechanism is at play in other coastal  
378 ice rises/domes at different times during the last deglaciation.

379

380 We previously had two proxies for ice sheet elevation, water isotopes and TAC, neither of which are perfect but have worked  
381 together in a “belts and braces” approach. Now we have a third in the form of  $\delta^{15}\text{N}$ , which reflects the rate of thinning, and  
382 thus can use a “belts, braces and buttons” approach when identifying past periods of rapid ice sheet destabilisation. Where de-  
383 stabilisation of the firnification process exists, the large magnitude oscillating TAC record measured in Skytrain ice core is not  
384 a true elevation signal. However, the nitrogen isotope record can be used to precisely identify the disrupted portion of the TAC  
385 record, helping to resolve the true elevation signal. Nitrogen isotopes are thus important to measure in future studies where  
386 TAC is being applied, particularly in regions such as coastal ice-rises where more rapid changes in ice mass are possible. TAC  
387 is still a powerful tool for relative elevation change estimates over rapid ice mass changes where disrupted records can be  
388 precisely identified and avoided, and indeed the combination with nitrogen isotopes opens the potential to constrain dynamic  
389 ice changes, subsequently informing model physics. Future work is planned for ice grain microstructure analysis to further  
390 investigate causes of the oscillations in the TAC signal, which is likely driven by an interplay of controls affecting pore volume  
391 in the firn column during bubble close-off.

392 **References**

393 Bender, M., Sowers, T., and Lipenkov, V.: On the concentrations of O<sub>2</sub>, N<sub>2</sub>, and Ar in trapped gases from ice cores, *J Geophys*  
394 *Res*, 100, <https://doi.org/10.1029/94jd02212>, 1995.

395 Calonne, N., Milliancourt, L., Burr, A., Philip, A., Martin, C. L., Flin, F., and Geindreau, C.: Thermal Conductivity of Snow,  
396 Firn, and Porous Ice From 3-D Image-Based Computations, *Geophys Res Lett*, 46, 13079–13089,  
397 <https://doi.org/10.1029/2019GL085228>, 2019.



398 Eicher, O., Baumgartner, M., Schilt, A., Schmitt, J., Schwander, J., Stocker, T. F., and Fischer, H.: Climatic and insolation  
399 control on the high-resolution total air content in the NGRIP ice core, *Climate of the Past*, 12, 1979–1993,  
400 https://doi.org/10.5194/cp-12-1979-2016, 2016.

401 Epifanio, J. A., Brook, E. J., Buzert, C., Pettit, E. C., Edwards, J. S., Fegyveresi, J. M., Sowers, T. A., Severinghaus, J. P., and  
402 Kahle, E. C.: Millennial and orbital-scale variability in a 54,000-year record of total air content from the South Pole ice core,  
403 *Cryosphere*, 17, 4837–4851, https://doi.org/10.5194/tc-17-4837-2023, 2023.

404 Fudge, T. J., Steig, E. J., Markle, B. R., Schoenemann, S. W., Ding, Q., Taylor, K. C., McConnell, J. R., Brook, E. J., Sowers,  
405 T., White, J. W. C., Alley, R. B., Cheng, H., Clow, G. D., Cole-Dai, J., Conway, H., Cuffey, K. M., Edwards, J. S., Lawrence  
406 Edwards, R., Edwards, R., Fegyveresi, J. M., Ferris, D., Fitzpatrick, J. J., Johnson, J., Hargreaves, G., Lee, J. E., Maselli, O.  
407 J., Mason, W., McGwire, K. C., Mitchell, L. E., Mortensen, N., Neff, P., Orsi, A. J., Popp, T. J., Schauer, A. J., Severinghaus,  
408 J. P., Sigl, M., Spencer, M. K., Vaughn, B. H., Voigt, D. E., Waddington, E. D., Wang, X., and Wong, G. J.: Onset of deglacial  
409 warming in West Antarctica driven by local orbital forcing, *Nature*, 500, 440–444, https://doi.org/10.1038/nature12376, 2013.

410 Greene, C. A., Gwyther, D. E., and Blankenship, D. D.: Antarctic Mapping Tools for MATLAB, *Comput Geosci*, 104, 151–  
411 157, https://doi.org/10.1016/j.cageo.2016.08.003, 2017.

412 Gregory, S. A., Albert, M. R., and Baker, I.: Impact of physical properties and accumulation rate on pore close-off in layered  
413 firn, *Cryosphere*, 8, 91–105, https://doi.org/10.5194/tc-8-91-2014, 2014.

414 Grieman, M. M., Nehrbass-Ahles, C., Hoffmann, H. M., Bauska, T. K., King, A. C. F., Mulvaney, R., Rhodes, R. H., Rowell,  
415 I. F., Thomas, E. R., and Wolff, E. W.: Abrupt Holocene ice loss due to thinning and ungrounding in the Weddell Sea  
416 Embayment, *Nat Geosci*, 17, 227–232, https://doi.org/10.1038/s41561-024-01375-8, 2024.

417 Herron, M. M. and Langway, C. C.: Firn Densification: An Empirical Model, *Journal of Glaciology*, 25, 373–385,  
418 https://doi.org/10.3189/s0022143000015239, 1980.

419 Hoffmann, H. M., Grieman, M. M., King, A. C. F., Epifanio, J. A., Martin, K., Vladimirova, D., Pryer, H. V., Doyle, E.,  
420 Schmidt, A., Humby, J. D., Rowell, I. F., Nehrbass-Ahles, C., Thomas, E. R., Mulvaney, R., and Wolff, E. W.: The ST22  
421 chronology for the Skytrain Ice Rise ice core - Part 1: A stratigraphic chronology of the last 2000 years, *Climate of the Past*,  
422 18, 1831–1847, https://doi.org/10.5194/cp-18-1831-2022, 2022.

423 Horlings, A. N., Christianson, K., Holschuh, N., Stevens, C. M., and Waddington, E. D.: Effect of horizontal divergence on  
424 estimates of firn-air content, *Journal of Glaciology*, 67, 287–296, https://doi.org/10.1017/jog.2020.105, 2021.

425 King, A. C. F., Bauska, T. K., Brook, E. J., Kalk, M., Nehrbass-Ahles, C., Wolff, E. W., Strawson, I., Rhodes, R. H., and  
426 Osman, M. B.: Reconciling ice core CO<sub>2</sub> and land-use change following New World-Old World contact, *Nat Commun*, 15,  
427 https://doi.org/10.1038/s41467-024-45894-9, 2024.

428 Kingslake, J., Scherer, R. P., Albrecht, T., Coenen, J., Powell, R. D., Reese, R., Stansell, N. D., Tulaczyk, S., Wearing, M. G.,  
429 and Whitehouse, P. L.: Extensive retreat and re-advance of the West Antarctic Ice Sheet during the Holocene, *Nature*, 558,  
430 430–434, https://doi.org/10.1038/s41586-018-0208-x, 2018.



431 Lliboutry, L.: A critical review of analytical approximate solutions for steady state velocities and temperatures in cold ice  
432 sheets, *Z. Gletscherde. Glazialgeol.*, 15, 135–148, 1979.

433 Martinerie, P., Raynaud, D., Etheridge, D. M., Barnola, J. M., and Mazaudier, D.: Physical and climatic parameters which  
434 influence the air content in polar ice, *Earth Planet Sci Lett*, 112, 1–13, [https://doi.org/10.1016/0012-821X\(92\)90002-D](https://doi.org/10.1016/0012-821X(92)90002-D), 1992.

435 Morgan, J. D., Buizert, C., Fudge, T. J., Kawamura, K., Severinghaus, J. P., and Trudinger, C. M.: Gas isotope thermometry  
436 in the South Pole and Dome Fuji ice cores provides evidence for seasonal rectification of ice core gas records, *Cryosphere*, 16,  
437 2947–2966, <https://doi.org/10.5194/tc-16-2947-2022>, 2022.

438 Morlighem, M., Rignot, E., Binder, T., Blankenship, D., Drews, R., Eagles, G., Eisen, O., Ferraccioli, F., Forsberg, R.,  
439 Fretwell, P., Goel, V., Greenbaum, J. S., Gudmundsson, H., Guo, J., Helm, V., Hofstede, C., Howat, I., Humbert, A., Jokat,  
440 W., Karlsson, N. B., Lee, W. S., Matsuoka, K., Millan, R., Mouginot, J., Paden, J., Pattyn, F., Roberts, J., Rosier, S., Ruppel,  
441 A., Seroussi, H., Smith, E. C., Steinhage, D., Sun, B., Broeke, M. R. van den, Ommen, T. D. van, Wessem, M. van, and Young,  
442 D. A.: Deep glacial troughs and stabilizing ridges unveiled beneath the margins of the Antarctic ice sheet, *Nat Geosci*, 13,  
443 132–137, <https://doi.org/10.1038/s41561-019-0510-8>, 2020.

444 Mulvaney, R., Rix, J., Polfrey, S., Grieman, M., Martin, C., Nehrbass-Ahles, C., Rowell, I., Tuckwell, R., and Wolff, E.: Ice  
445 drilling on Skytrain Ice Rise and Sherman Island, Antarctica, *Ann Glaciol*, 62, 311–323, <https://doi.org/10.1017/aog.2021.7>,  
446 2021.

447 Mulvaney, R., Wolff, E. W., Grieman, M. M., Hoffmann, H. H., Humby, J. D., Nehrbass-Ahles, C., Rhodes, R. H., Rowell, I.  
448 F., Parrenin, F., Schmidely, L., Fischer, H., Stocker, T. F., Christl, M., Muscheler, R., Landais, A., and Prié, F.: The ST22  
449 chronology for the Skytrain Ice Rise ice core – Part 2: An age model to the last interglacial and disturbed deep stratigraphy,  
450 *Climate of the Past*, 19, 851–864, <https://doi.org/10.5194/cp-19-851-2023>, 2023.

451 Nehrbass-Ahles, C., King, A., Hoffmann, H., Grieman, M., Rowell, I., Humby, J., Miller, S., Thomas, E., Bauska, T., Schmitt,  
452 J., Mulvaney, R., and Wolff, E.: A high-accuracy Total Air Content setup: System performance and first results from Skytrain  
453 Ice Rise, Antarctica, *EGU General Assembly 2022*, Vienna, Austria, 23–27 May 2022, EGU22-9210,  
454 <https://doi.org/10.5194/egusphere-egu22-9210>, 2022.

455 Nicola, L., Notz, D., and Winkelmann, R.: Revisiting temperature sensitivity: how does Antarctic precipitation change with  
456 temperature?, *Cryosphere*, 17, 2563–2583, <https://doi.org/10.5194/tc-17-2563-2023>, 2023.

457 Oraschewski, F. M. and Grinsted, A.: Modeling enhanced firn densification due to strain softening, *Cryosphere*, 16, 2683–  
458 2700, <https://doi.org/10.5194/tc-16-2683-2022>, 2022.

459 Pittard, M. L., Whitehouse, P. L., Bentley, M. J., and Small, D.: An ensemble of Antarctic deglacial simulations constrained  
460 by geological observations, *Quat Sci Rev*, 298, <https://doi.org/10.1016/j.quascirev.2022.107800>, 2022.

461 Pörtner, H., Roberts, D., Poloczanska, E., Mintenbeck, K., Tignor, M., and Alegria, A.: *IPCC Sixth Assessment Report*,  
462 Cambridge University Press, 2022.



463 Rhodes, R. H., Brook, E. J., Chiang, J. C. H., Blunier, T., Maselli, O. J., McConnell, J. R.,; Romanini, D., Severinghaus, J. P.:  
464 Enhanced tropical methane production in response to iceberg discharge in the North Atlantic. *Science*, 348(6238), 1016-1019,  
465 <https://doi.org/10.1126/science.1262005>, 2015.

466 Rosser, J. P., Winkelmann, R., and Wunderling, N.: Polar ice sheets are decisive contributors to uncertainty in climate tipping  
467 projections, *Commun Earth Environ*, 5, <https://doi.org/10.1038/s43247-024-01799-5>, 2024.

468 Servettaz, A. P. M., Orsi, A. J., Curran, M. A. J., Moy, A. D., Landais, A., McConnell, J. R., Popp, T. J., Le Meur, E., Faïn,  
469 X., and Chappelaz, J.: A 2000-year temperature reconstruction on the East Antarctic plateau, from argon-nitrogen and water  
470 stable isotopes in the Aurora Basin North ice core, <https://doi.org/10.5194/cp-2022-91>, 20 December 2022.

471 Severinghaus, J. P., Grachev, A., Luz, B., and Caillon, N.: A method for precise measurement of argon 40/36 and krypton/argon  
472 ratios in trapped air in polar ice with applications to past firn thickness and abrupt climate change in Greenland and at Siple  
473 Dome, Antarctica, 2003.

474 Severinghaus, J. P., Beaudette, R., Headley, M. A., Taylor, K., and Brook, E. J.: Oxygen-18 of O<sub>2</sub> Records the Impact of  
475 Abrupt Climate Change on the Terrestrial Biosphere, *Science* (1979), 324, 1431–1434,  
476 <https://doi.org/10.1126/science.1169473>, 2009.

477 Spector, P., Stone, J., Cowdery, S. G., Hall, B., Conway, H., and Bromley, G.: Rapid early-Holocene deglaciation in the Ross  
478 Sea, Antarctica, *Geophys Res Lett*, 44, 7817–7825, <https://doi.org/10.1002/2017GL074216>, 2017.

479 Stevens, C. M., Verjans, V., Lundin, J. M. D., Kahle, E. C., Horlings, A. N., Horlings, B. I., and Waddington, E. D.: The  
480 Community Firn Model (CFM) v1.0, *Geosci Model Dev*, 13, 4355–4377, <https://doi.org/10.5194/gmd-13-4355-2020>, 2020.

## 481 **Data Availability**

482 Data published in this manuscript will be uploaded to the PANGEA data repository on acceptance of the manuscript.

## 483 **Author Contributions**

484 A.C.F.K: Project concept, sample preparation, data interpretation, wrote manuscript, revised manuscript. T.K.B: data  
485 interpretation, wrote manuscript, revised manuscript, funded sample analysis. A.L: Sample analysis, data interpretation,  
486 revised manuscript. C.M: Data interpretation, revised manuscript. E.W. Collected and supplied samples, revised manuscript.



487 **Competing Interests**

488 At least one of the (co-)authors is a member of the editorial board of Climate of the Past.

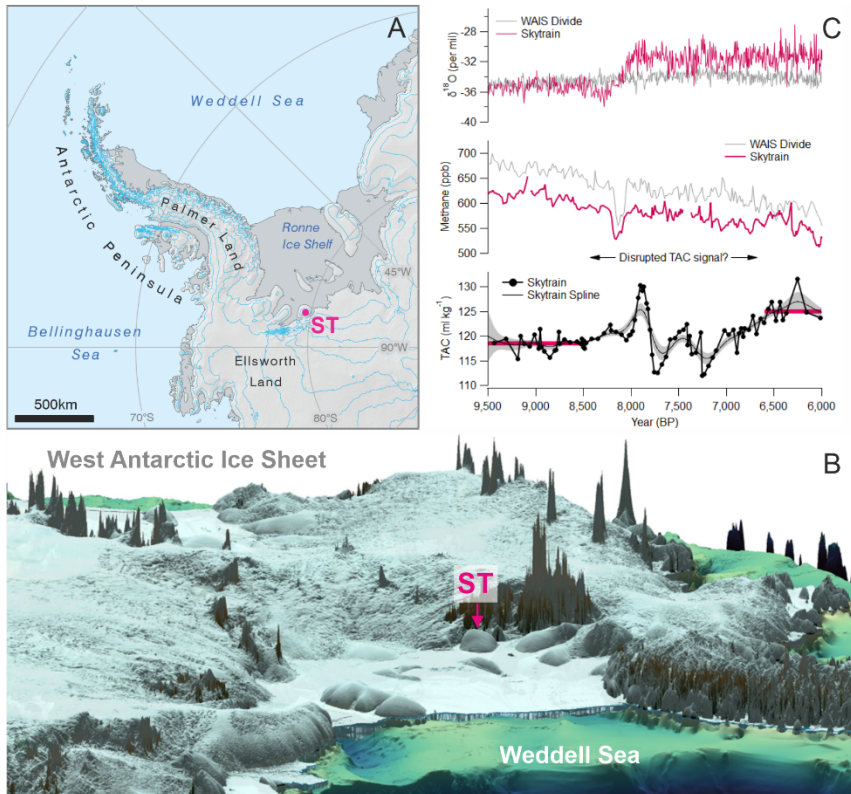
489 **Acknowledgements**

490 The authors would like to thank Frédéric Prié and Elodie Brugère for their contribution to the measurements of the ice core  
491 samples at the lab in LSCE, Paris and all those involved in the Skytrain Ice Core project. This project has received funding  
492 from the European Research Council under the Horizon 2020 research and innovation programme (grant agreement no.  
493 742224, WACSWAIN, held by E.W.W). This material reflects only the authors' views and the Commission is not liable for  
494 any use that may be made of the information contained therein. The work was additionally supported by Royal Society Grants  
495 URF\R1\180366 and RGF\EA\181047 held by T.K.B.

496



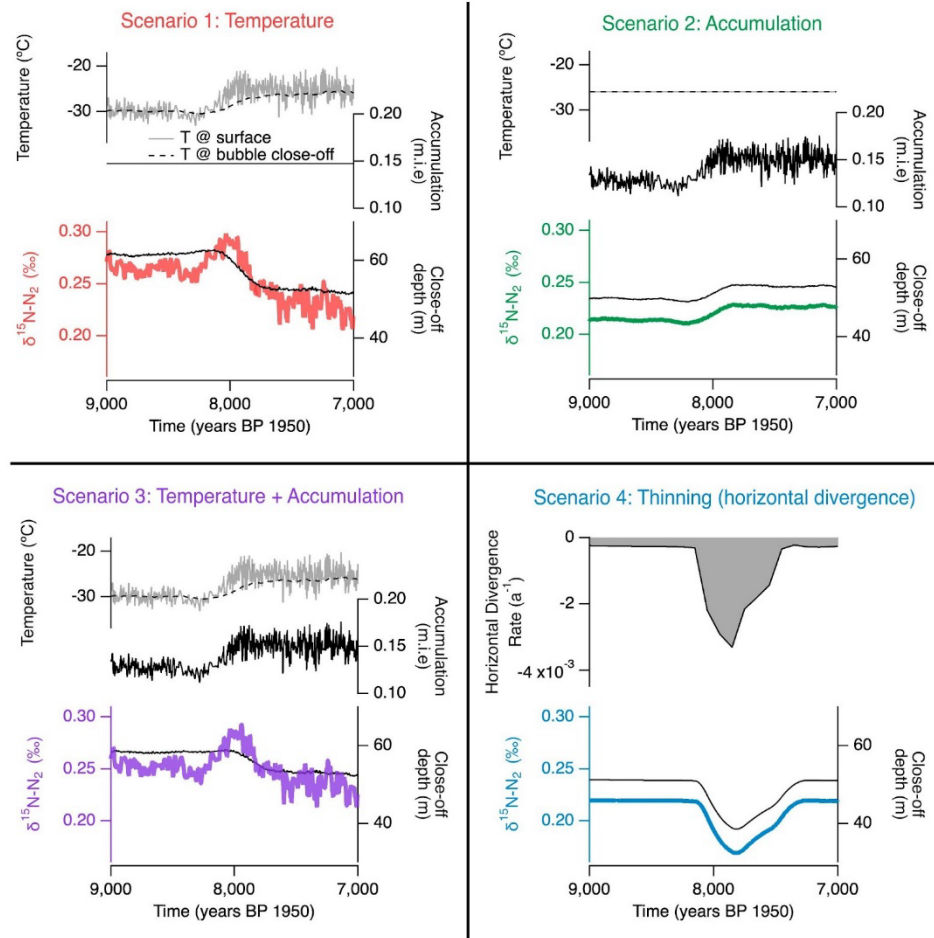
497



498

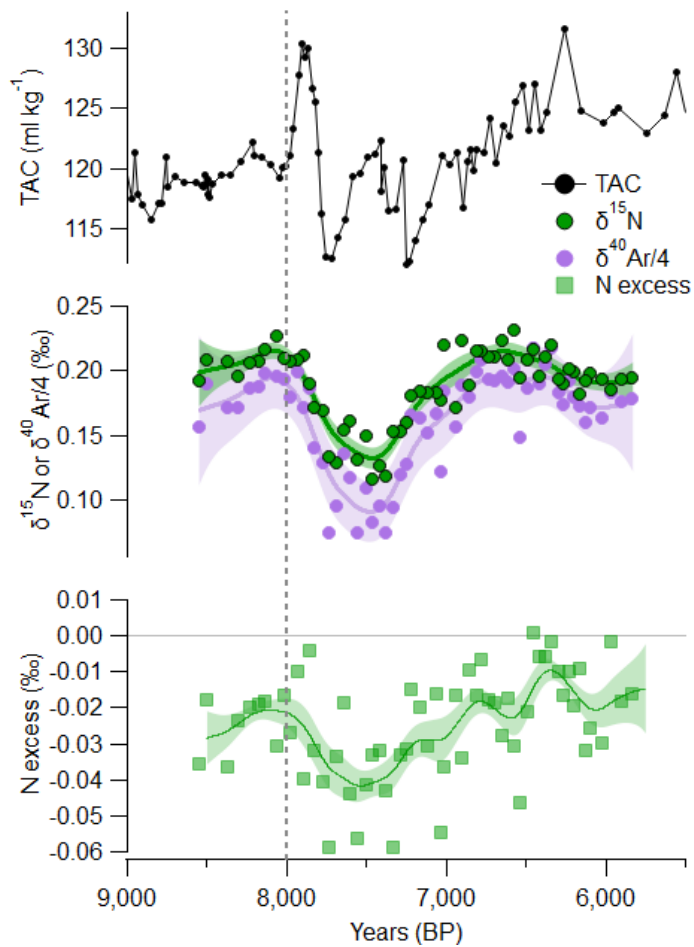
499

500 **Figure 1: Location map of Skytrain Ice Rise (panel A, 'ST') and shown in a 3D topographic context (panel B, Greene  
501 et al., 2017; Morlighem et al., 2020) with ST sitting at the interface between the floating Ronne Ice Shelf and the outward  
502 flowing continental ice sheet of West Antarctica. Panel C highlights the elevation loss event, over ~ 200 years at ~8 ka,  
503 observed in the Skytrain ice core records, with a significant jump in water isotopes caused by ice elevation loss and  
504 subsequent temperature increase at the site (Grieman et al., 2024). Comparatively, records from the central WAIS,  
505 indicated by the WAIS Divide ice core record (Fudge et al., 2013), remain relatively stable. The TAC record from  
506 Skytrain, which is expected to indicate elevation at SIR during the ice mass change, shows a complex oscillating signal  
507 after 8 ka which is too great to be an elevation signal, and does not re-stabilise until significantly later, ~6.5 ka. Also  
508 shown are the CH<sub>4</sub> record from Skytrain and WAIS Divide (Rhodes et al., 2015; Buzert et al., 2015).  
509**



510

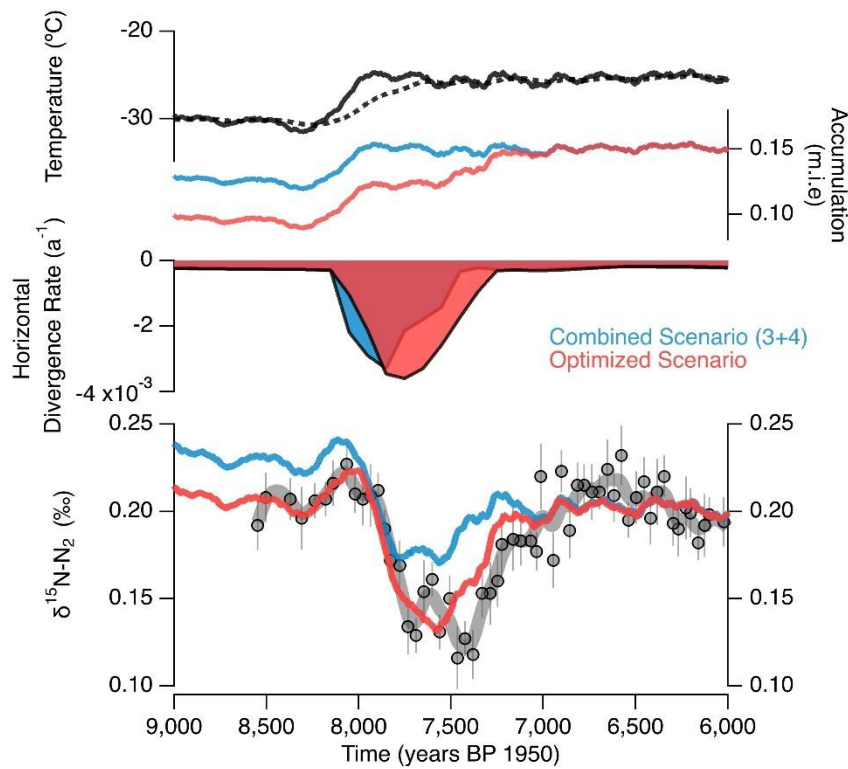
511 **Figure 2: Factorial Experiments using the CFM to disentangle the potential drivers of  $\delta^{15}\text{N}$  variability at SIR.** Panels  
512 show changes in temperature-only (red), accumulation-only (green) and a combination of temperature and  
513 accumulation (purple) with the two forcings of surface temperature (light grey) and accumulation (solid black). Also  
514 shown in these panels are the predicted temperature at bubble close-off (dashed black), the close-off depth (solid black)  
515 and the  $\delta^{15}\text{N}$  (coloured coded to the given experiment). Panel 4 shows the prediction using just the horizontal divergence  
516 calculated from PISM plus constant accumulation rate (filled in grey).



517

518

519 **Figure 3:** Values of  $\delta^{15}\text{N}$  and  $\delta^{40}\text{Ar}$  from the Skytrain ice core (middle panel) throughout the rapid elevation change at  
520 the site  $\sim 8$  ka (dashed line), plotted against the previously published TAC data (top panel) (Grieman et al., 2024).  
521 Smoothing splines are also presented (see methods), with uncertainty bands becoming large at the ends of the dataset  
522 due to a lack of constraining data points beyond here. Also shown is the calculated N excess.  
523



524

525 **Figure 4: Optimising the model parameters to best fit data, where accumulation and horizontal divergence rates are**  
526 **adjusted so that the model output of the absolute values of  $\delta^{15}\text{N}$  and duration of the reduction in  $\delta^{15}\text{N}$  more closely**  
527 **match the measured data ('Optimised scenario', lower panel).**

528

529

530

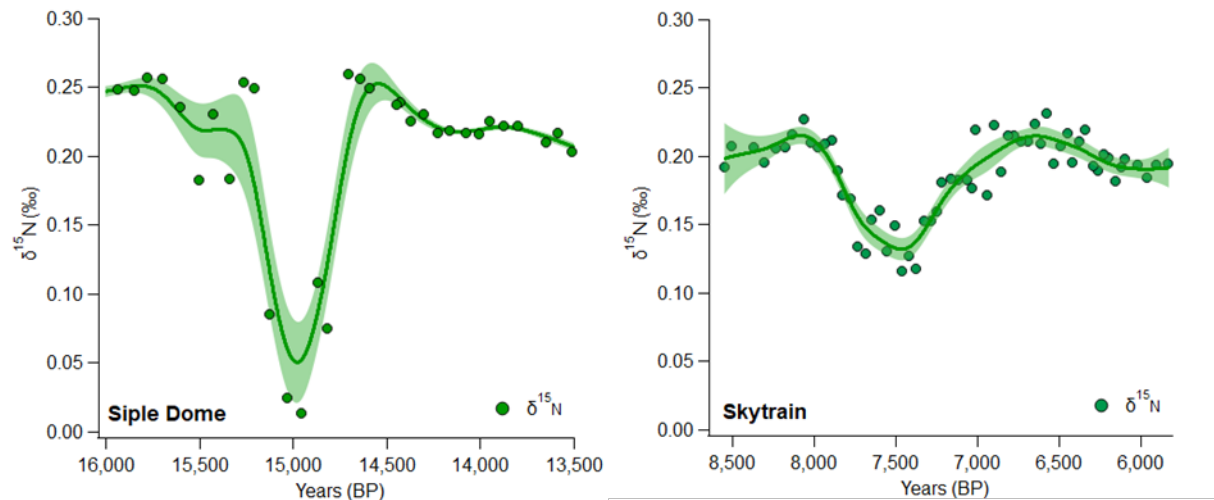
531

532

533

534

535



536

537 **Figure 5: Comparison of  $\delta^{15}\text{N}$  from the Siple Dome (left) (Severinghaus et al., 2003, 2009) and Skytrain (right)**,  
538 **highlighting the substantial drop in  $\delta^{15}\text{N}$  in both records lasting over timescales of  $\sim 1000$  years.**

539

540

541

542

543

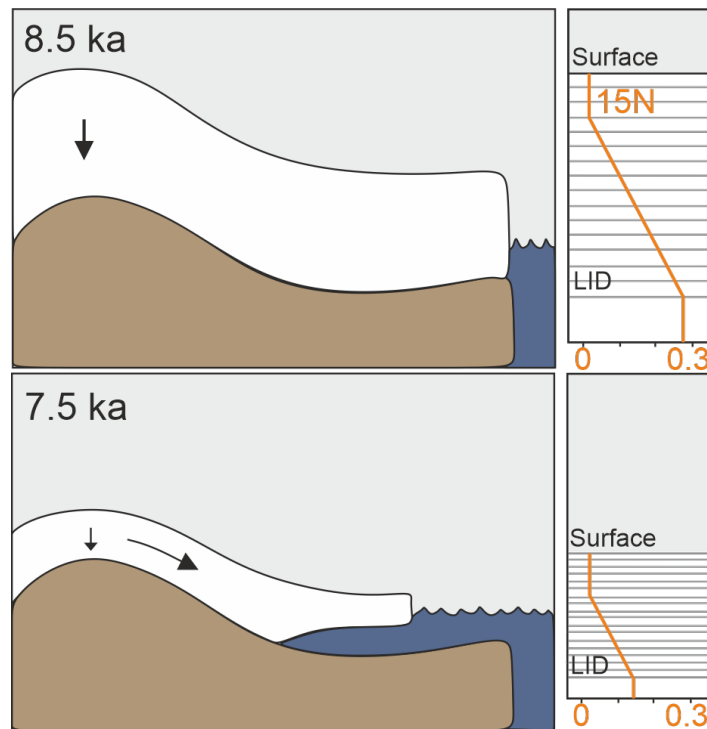
544

545

546

547

548



549

550 **Figure 6: Schematic of the physical ice changes at Skytrain Ice Rise throughout the 8 ka elevation change alongside the**  
551 **effects on the  $\delta^{15}\text{N}$  values shown as profiles through the respective firn column for each scenario of ice thickness. Where**  
552 **ice dynamics are stable at 8.5 ka,  $\delta^{15}\text{N}$  increases down the firn column from the ice surface to bubble lock-in depth**  
553 **(LID) due to gravitational fractionation. Where ice thickness is reduced and layers dynamically thinned due to**  
554 **horizontal divergence at 7.5 ka, there is less gravitational fractionation through the thinned firn-column, resulting in**  
555 **lower values of captured  $\delta^{15}\text{N}$  at bubble LID. Values of  $\delta^{15}\text{N}$  shown here are indicative only.**

556

557

558